Microstructures

Research Article

Structure, magnetism and low thermal expansion in Tb$_{1-x}$Er$_x$Co$_2$Mn$_y$ intermetallic compounds

Yanming Sun[1], Yili Cao[1], Yang Ren[2], Saul H. Lapidus[3], Qiang Li[1], Jinxia Deng[1], Jun Miao[1], Kun Lin[1], Xianran Xing[1] iD

[1]Beijing Advanced Innovation Center for Materials Genome Engineering, Institute of Solid State Chemistry, Department of Physical Chemistry, University of Science and Technology Beijing, Beijing 100083, China.
[2]Department of Physics, City University of Hong Kong, Kowloon, Hong Kong, China.
[3]X-Ray Science Division, Argonne National Laboratory, Argonne, IL 60439, USA.

Correspondence to: Prof. Xianran Xing, Department of Physical Chemistry, University of Science and Technology Beijing, Xueyuan Rd. 30, Haidian District, Beijing 100083, China. E-mail: xing@ustb.edu.cn

Abstract

Here, we obtained a series of controllable thermal expansion alloys Tb$_{1-x}$Er$_x$Co$_2$Mn$_y$ (x = 0-0.5, y = 0-0.4) by incorporating double rare earth doping and introducing non-stoichiometric Mn content. By varying the amount of Er or Mn, a low thermal expansion (LTE) is achieved in Tb$_{0.6}$Er$_{0.4}$Co$_2$Mn$_{0.1}$ (TECM, α_1 = 1.23 × 10^{-6} K^{-1}, 125~236 K). The macroscopic linear expansion and magnetic properties reveal that anomalous thermal expansion is closely related to the magnetic phase transition. Synchrotron X-ray powder diffraction results show that TECM is a cubic phase (space group: Fd-3m) at high temperatures, and a structural transition to a rhombohedral phase (space group: R-3m) occurs as temperature decreases. The negative thermal expansion c-axis compensates for the normal positive thermal expansion of the basal plane, resulting in the volumetric LTE. This study provides a new metallic and magnetic ZTE material.

Keywords: Zero thermal expansion, crystal structure, microstructure, magnetism

INTRODUCTION

By flexibly compensating for thermal expansion, negative thermal expansion (NTE) materials have gained

significant attention and development over the past three decades. The NTE is an important requirement for the development of zero thermal expansion (ZTE) materials, which exhibit no dimensional changes when subjected to heating. Materials with a coefficient of thermal expansion below 2×10^{-6} K^{-1} are defined as low thermal expansion (LTE) materials and find applications in various engineering environments, such as electronic devices, optical instruments, and spacecraft. An example is Invar alloy $Fe_{0.65}Ni_{0.35}$, which has been extensively used since its discovery in 1897[1]. Over time, other LTE alloys such as Fe-Co-Cr stainless steel Invar alloys and other alloy compositions have emerged[2]. In comparison with oxides[3], fluorides[4], and cyanides[5], LTE alloys offer additional properties such as optical properties[6], excellent electrical, thermal transport properties, and mechanical properties[7-9]. Examples of such alloys include $(Zr, Nb)Fe_2$[10,11], $(Sc, Ti)Fe_2$[12], $MnCoGe$[13,14], $La(Fe, Si, Al)_{13}$[15,16], $RECo_2$ (RE = rare earth)[17,18], $REFe_{14}B$[19], and RE_2Fe_{17}[20,21]. The metallic ZTE is known to be correlated with the magneto-volume effect (MVE), which refer to volume changes induced by spontaneous magnetic ordering[16,22].

Cubic Laves phase $RECo_2$ has been studied intensively due to its relatively simple crystal and magnetic structures. It belongs to a class of materials known for their magnetostrictive and magnetocaloric properties[23]. The compound is composed of two magnetic sublattices: one involving the local magnetic moment of REs, and the other comprising the Co sublattice, which exhibits long-range magnetic ordering induced by the molecular field of RE atoms[24,25]. In previous literature, samples $TbCo_2Mn_y$ (y = 0, 0.1, 0.2, and 0.3) were found to exhibit a rhombohedral structure (space group: R-$3m$) below the Curie temperature (T_C) and undergo a transition to a cubic structure (space group: Fd-$3m$) above T_C[26]. $TbCo_2Mn_y$ were reported for the ZTE temperature window of about 40 K[23]. Intriguingly, the introduction of the element Er in compound $TbCo_2Mn_y$ gives the Laves phase of $Tb_{1-x}Er_xCo_2Mn_y$, and their ZTE temperature windows can be wider with increasing Er content. In the $(RE_{1-x}RE'_x)(Co_{1-y}M_y)_2$ compounds, the substitution of the RE' atoms for the RE atoms occurs only in the 16d atomic site, while the substitution of the M atoms for Co atoms takes place in the 8a site[24]. This differs from the $(RE_{1-x}RE'_x)Co_2Mn_y$ compounds, where the Mn atoms can replace the 8a and 16d sites in the cubic structure with equal probability[27]. This unusual modulation of multiple sites in $(RE_{1-x}RE'_x)Co_2Mn_y$ compounds significantly increases the T_C of the corresponding Mn-free compounds. In this study, new intermetallic compounds $Tb_{1-x}Er_xCo_2Mn_y$ (x = 0, 0.1, 0.2, 0.4, and 0.5, y = 0 and 0.1), with a $MgCu_2$ type cubic structure, are introduced. These compounds can be modulated by changing their components to achieve near ZTE.

MATERIALS AND METHODS

All the Laves-phase samples of $Tb_{1-x}Er_xCo_2Mn_y$ (x = 0, 0.1, 0.2, 0.4, and 0.5, y = 0 and 0.1) were prepared by arc melting under high-purity argon environment using raw materials with a purity of more than 99.9%, which were weighed at the designed ratio of raw materials. To ensure homogeneity, the samples were turned over and melted more than three times. At the end of the arc melting, the ingots are wrapped with molybdenum foil and annealed in a vacuum-sealed quartz tube at 1,173 K for one week. The purity of the samples was verified by a laboratory X-ray diffractometer (XRD, PANalytical X'Pert PRO) with Cu Kα radiation. The scanning electron microscopy (SEM) imaging and X-ray energy dispersive spectroscopy (EDS) elemental analysis were performed using a scanning electron microscope system (1,720, EPMA, Shimadzu). All linear thermal expansion curves ($\Delta L/L_0$) were measured at a thermodilatometer (NETZSCH DIL402) with a heating rate of 5 K/min. The magnetic properties were measured by a Physical Property Measurement System (PPMS, Quantum Design company). Temperature dependence of the synchrotron X-ray diffraction (SXRD) of the sample was collected at beamline of 11-BM-B (λ = 0.459073 Å) in the Argonne National Laboratory (USA). All diffraction data were analyzed by the FULLPROF software.

RESULTS AND DISCUSSION

$Tb_{1-x}Er_xCo_2Mn_y$ (x = 0, 0.1, 0.2, 0.4, and 0.5, y = 0, 0.1, 0.2, 0.3) were confirmed to be pure phases by XRD at room temperature (except y = 0.4). For example, at 300 K, the Rietveld refinement of the SXRD data for $Tb_{0.6}Er_{0.4}Co_2Mn_{0.1}$ (denoted as TECM) shows the cubic structure in Supplementary Figure 1. In $Tb_{1-x}Er_xCo_2$ (x = 0, 0.1, 0.2, 0.4, and 0.5, Figure 1A and B: It is cubic without Er (x = 0, $TbCo_2$) and remains cubic with increasing Er content (x ≤ 0.5). Meanwhile, it was observed that the peak (220) shifted to a higher angle due to the successful introduction of smaller radii Er atoms. In $Tb_{1-x}Er_xCo_2Mn_{0.1}$ (x = 0, 0.1, 0.2, 0.4, and 0.5), the peak (220) shifted to a high angle with increasing Er content, while the Mn content being fixed at y = 0.1 and still maintaining the cubic phase)[Figure 1C and D]. To investigate the effect of different Er contents on $Tb_{1-x}Er_xCo_2$ and $Tb_{1-x}Er_xCo_2Mn_{0.1}$, the cell parameters of which were obtained by fitting the XRD data [Supplementary Figure 2 and Supplementary Table 1]. In addition, we successfully synthesized $Tb_{0.6}Er_{0.4}Co_2Mn_y$ (y = 0, 0.1, 0.2, 0.3, and 0.4) with increasing Mn content. The samples have a similar cubic structure below y = 0.4 [Supplementary Figure 3]. The cubic structure of the $RECo_2$ is shown in Figure 1F. The rhombohedral structure is also presented in Figure 1E as the temperature decreases below T_C. The SEM images and EDS elemental mappings shown in Figure 1G-K and Supplementary Table 2 illustrate the uniform distribution of elements Tb, Er, Co, and Mn in TECM (Tb:Er:Co:Mn = 0.58:0.37:2:0.09). The contents of Co and Mn were close to the nominal compositions, as evidenced by the ICP results shown in Supplementary Table 3.

As shown in Figure 2, the samples $Tb_{1-x}Er_xCo_2Mn_y$ (x = 0, 0.1, 0.2, 0.4, and 0.5, y = 0 and 0.1) exhibit a significantly different linear thermal expansion behavior. The NTE behavior of $TbCo_2$ occurs in a narrow temperature window. Interestingly, the anomalous thermal expansion of the $Tb_{1-x}Er_xCo_2$ (x = 0, 0.1, 0.2, and 0.4) compounds ends at lower temperatures with increasing Er content. A large NTE coefficient of $Tb_{0.6}Er_{0.4}Co_2$ (denoted as TEC, α_l = -15.29 × 10^{-6} K^{-1}, 131-167 K) was obtained [Figure 2A]. To obtain LTE, the ferromagnetic (FM) exchange interactions can be enhanced by introducing Mn atoms at the Tb/Er $8a$ and Co $16d$ sites[28]. However, the samples $Tb_{1-x}Er_xCo_2Mn_{0.1}$ (x = 0, 0.1, 0.2, 0.4, and 0.5) [Figure 2B], are different from the above. As Er replaces Tb, the volume shrinkage behavior of $Tb_{1-x}Er_xCo_2Mn_{0.1}$ decreases, and the LTE temperature window of $Tb_{1-x}Er_xCo_2Mn_{0.1}$ gradually appears and expands to x = 0.4. The LTE is obtained with TECM (α_l = 1.23 × 10^{-6} K^{-1}, 125-236 K) when x = 0.4. For comparison, the coefficient of thermal expansion value of TECM is smaller than that of common metals such as Fe (α_l = 12.2(0) × 10^{-6} K^{-1}), Al (α_l = 22.9(0) × 10^{-6} K^{-1}), Cu (α_l = 16.3(1) × 10^{-6} K^{-1}), *etc*. However, the coefficient of thermal expansion trends from negative to positive with increasing Er content [Supplementary Figure 4]. TECM has a wide temperature window of the LTE curves, which may offer promising prospects for both basic research and applications.

The magnetic phase transition of $TbCo_2$ was documented to be first-order, while that of the $TbCo_2Mn_x$ compound obtained by the addition of Mn was second-order[23]. The addition of Mn significantly increased the T_C of the compounds, for example, from 225 K for $TbCo_2$ to 347 K for $TbCo_2Mn_{0.4}$[29]. The macroscopic FM behavior of $Tb_{1-x}Er_xCo_2Mn_y$ (x = 0, 0.1, 0.2, 0.4, and 0.5, y = 0 and 0.1) was determined by measurements of zero-field cooling (ZFC) and field cooling (FC) during heating in a 500 Oe magnetic field [Figure 3A and B]. It is obvious that the FM transition temperature of the compound TEC is 167 K [Figure 3C], and that of TECM is 236 K [Figure 3D]. In $Tb_{1-x}Er_xCo_2$ and $Tb_{1-x}Er_xCo_2Mn_{0.1}$ samples, the magnetic transition temperature shifts to the low temperature with increasing Er content. The above results can be obtained from the derivative curves of FC/ZFC. The introduction of Mn effectively increases the FM transition temperature, as shown by the curves of T_C in Figure 3E, which is essential for obtaining LTE materials with a wide-temperature window. To further verify the FM transition temperature, isothermal magnetization curves *M-H* for selected TEC and TECM are shown in Figures 3F and
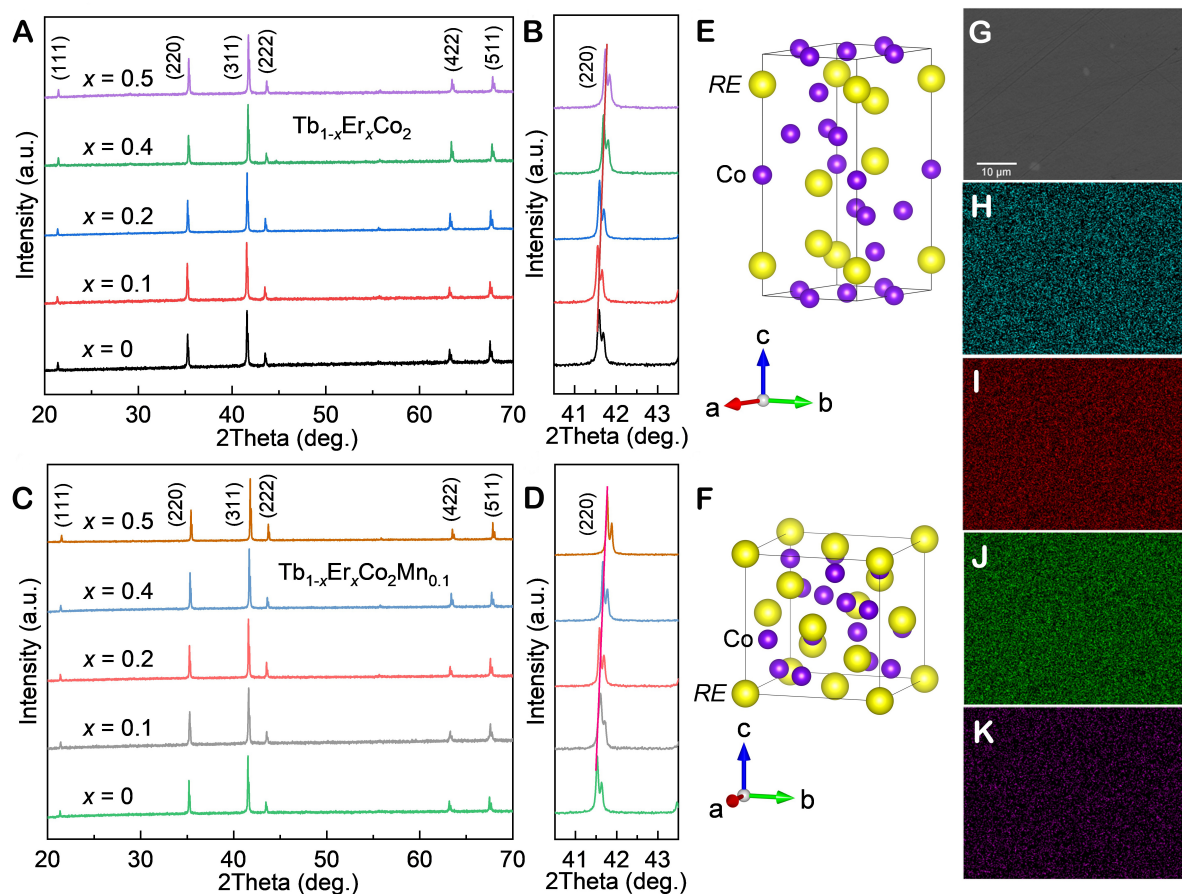
Figure 1. XRD patterns of the (A) $Tb_{1-x}Er_xCo_2$ (x = 0, 0.1, 0.2, 0.4, and 0.5) and (C) $Tb_{1-x}Er_xCo_2Mn_{0.1}$ (x = 0, 0.1, 0.2, 0.4, and 0.5). The corresponding enlarged diffraction peaks (220) are (B and D). The rhombohedral (E) and cubic (F) crystal structures of $RECo_2$ (RE = rare earth, the orange ball is RE, and the purple ball is Co). (G) The SEM images and EDS elemental mappings of (H) Tb, (I) Er, (J) Co, and (K) Mn of TECM, showing the uniformity of each element.
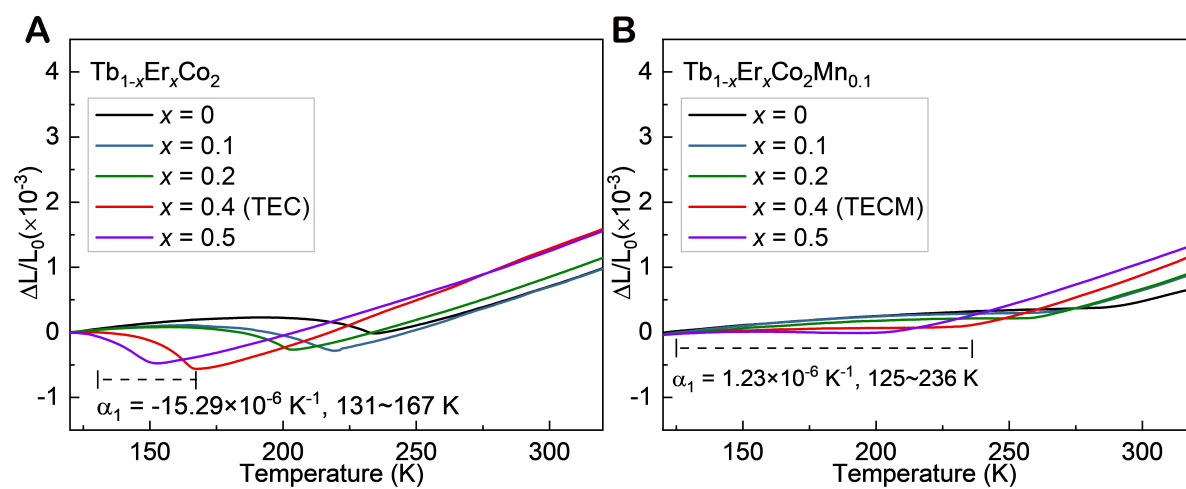
Figure 2. Linear thermal expansion ($\Delta L/L_0$) of (A) $Tb_{1-x}Er_xCo_2$ (x = 0, 0.1, 0.2, 0.4, and 0.5) and (B) $Tb_{1-x}Er_xCo_2Mn_{0.1}$ (x = 0, 0.1, 0.2, 0.4, and 0.5).
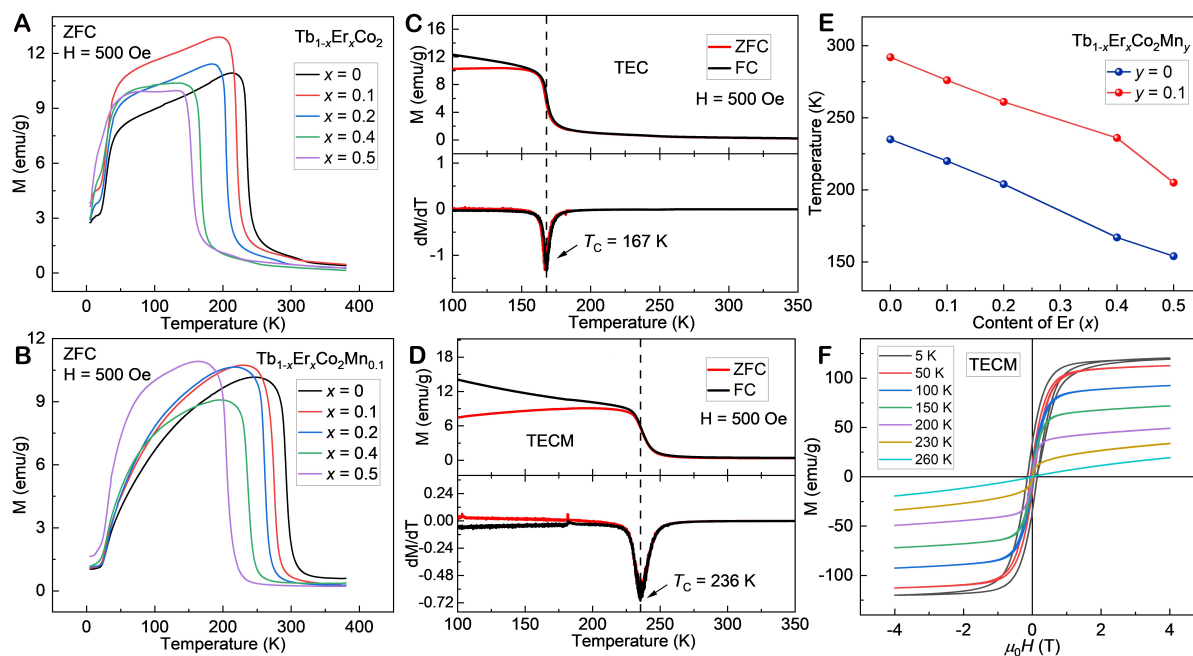
Figure 3. Temperature dependence of ZFC for the (A) $Tb_{1-x}Er_xCo_2$ and (B) $Tb_{1-x}Er_xCo_2Mn_{0.1}$ compounds under an applied magnetic field of 500 Oe from 5 to 380 K. FC-ZFC and the derivative curves of FC/ZFC of (C) TEC and (D) TECM compounds, respectively. (E) Curie temperature for $Tb_{1-x}Er_xCo_2Mn_y$ (the results are obtained from the derivative curves of FC/ZFC). (F) Isothermal *M-H* curves (-4 to 4 T) for TECM.

Supplementary Figure 5. The molecular magnetic moment of TEC is 6.32 μ_B/f.u., which is higher than that of TECM (6.10 μ_B/f.u.) at 5 K [Supplementary Figure 6]. As shown in Supplementary Figure 7, the introduction of Mn increases the phase transition temperature. A close correlation between structure, magnetic and thermal expansion. The crystal structural and magnetic transition temperature of TEC and TECM were found to be consistent with the point of the disappearance of NTE or ZTE, which would be helpful in plotting the curves of structural transition, ZFC-FC, and delta L/L$_0$ (T).

In the SXRD intensity contour plot of the TECM compound [Figure 4A], a splitting of the peak at low temperatures near 20.85° was found. The crystal structure of TECM was determined by SXRD, and it was demonstrated that it produces a phase transition from cubic (F*d*-3*m* space group) to rhombohedral (R-3*m* space group) with decreasing temperature. Rietveld refinement results of TECM at T = 100 K and T = 275 K are shown in Figure 4B. By a refinement of the SXRD pattern, this transition can be described in the inset of Figure 4B. The results show that the two peaks (110) and (104) of the rhombohedral structure are replaced by the peak (220) of the cubic structure. The temperature dependence of the unit lattice parameters and volume of TECM from 100 K to 325 K is shown in Figure 4C. From the correlation between the unit cell of the rhombohedral model (space group: R-3*m*) and the cubic model (space group: F*d*-3*m*), it is clear that the amounts of $\sqrt{2}a$ and $c/\sqrt{3}$ (a and c are the lattice parameters of the rhombohedral) are equivalent to the cubic amounts[30]. From thermodilatometer measurement and SXRD calculation results [Figure 4C], it is clear that the linear thermal expansion of TECM is consistent.

CONCLUSIONS

In summary, a series of $Tb_{1-x}Er_xCo_2Mn_y$ intermetallic compounds with a cubic $MgCu_2$-type structure were synthesized. The addition of Mn increases the T_C and contributes to a low thermal expansion with a wide temperature window. It has been confirmed by the high-resolution SXRD, which signifies such LTE is
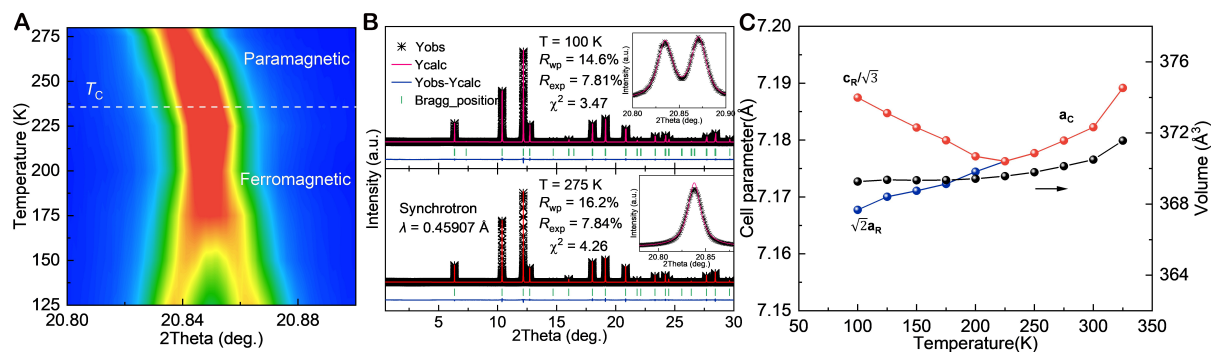
Figure 4. (A) Contour plot of the SXRD intensity for TECM compound. (B) Full profile Rietveld refinements of the SXRD patterns for the TECM compound at 100 K and 275 K. (The illustration shows the enlarged area. The experimental profiles are shown by star markers. Bragg reflections are indicated by ticks. Pink lines represent the calculated data, while black lines represent the difference between the observed and calculated data.) (C) Temperature dependence of the lattice parameters $a, c,$ and V of TECM measured by SXRD. (The amounts of $\sqrt{2}a$ and $c/\sqrt{3}$ (a and c are the lattice parameters of the rhombohedra) are equivalent to the cubic amounts).

attributed to magnetic-structural transition below T_C. The TECM compound shows a cubic (Fd-3m) structure above T_C while transforming to rhomboidal (R-3m) below T_C. TECM has a wide temperature window of the low thermal expansion curves, which offers good prospects for both basic research and applications. This work provides structural information and near ZTE properties of the compounds $Tb_{1-x}Er_xCo_2Mn_y$, which may guide future exploration of magnetic functional materials.

DECLARATIONS

Authors' contributions
Conceived and designed the study: Xing X
Prepared the samples and collected the data: Sun Y
Performed data analysis and wrote the main draft of the paper: Sun Y, Cao Y, Xing X
Analyzed the thermal expansion results: Li Q, Deng J, Miao J, Lin K
Conducted the SXRD measurements: Ren Y, Lapidus SH
All authors discussed the results and commented on the manuscript.

Availability of data and materials
Not applicable.

Conflicts of interest
All authors declared that there are no conflicts of interest.

Ethical approval and consent to participate
Not applicable.

Consent for publication

Not applicable.

Copyright

© The Author(s) 2023.

REFERENCES

1. Guillaume C. Recherches sur les aciers au nickel. *J Phys Theor Appl* 1898;7:262-74. DOI
2. Honda K. A new alloy, 'stainless-invar'. *Nature* 1933;131:587-587. DOI
3. Huang Q, Santoro A, Lynn JW, et al. Structure and magnetic order in $La_{1-x}Ca_xMnO_3$ ($0 < x < \sim0.33$). *Phys Rev B* 1998;58:2684-91. DOI
4. Li Q, Lin K, Liu Z, et al. Chemical diversity for tailoring negative thermal expansion. *Chem Rev* 2022;122:8438-86. DOI
5. Chippindale AM, Hibble SJ, Bilbé EJ, et al. Mixed copper, silver, and gold cyanides, $(M_xM'_{1-x})CN$: tailoring chain structures to influence physical properties. *J Am Chem Soc* 2012;134:16387-400. DOI
6. Poornaprakash B, Subramanyam K, Vattikuti SP, Pratap Reddy MS. Achieving enhanced ferromagnetism in ZnTbO nanoparticles through Cu co-doping. *Ceram Int* 2019;45:16347-52. DOI
7. Tan Z, Miao P, Hagihala M, et al. Room temperature zero thermal expansion in a cubic cobaltite. *J Phys Chem Lett* 2020;11:6785-90. DOI
8. Guo X, Ni X, Li J, et al. Designing mechanical metamaterials with kirigami-inspired, hierarchical constructions for giant positive and negative thermal expansion. *Adv Mater* 2021;33:e2004919. DOI
9. Xu J, Wang Z, Huang H, et al. Significant zero thermal expansion via enhanced magnetoelastic coupling in kagome magnets. *Adv Mater* 2023;35:e2208635. DOI
10. Song Y, Sun Q, Yokoyama T, et al. Transforming thermal expansion from positive to negative: the case of cubic magnetic compounds of $(Zr,Nb)Fe_2$. *J Phys Chem Lett* 2020;11:1954-61. DOI
11. Shiga M, Nakamura Y. Magnetovolume effects and invar characters of $(Zr_{1-x}Nb_x)Fe_2$. *J Phys Soc Jpn* 1979;47:1446-51. DOI
12. Wada H, Shimamura N, Shiga M. Thermal and transport properties of $Sc_{1-x}Ti_xFe_2$. *J Phys Soc Jpn* 1994;63:283-8. DOI
13. Ren Q, Hutchison W, Wang J, et al. Negative thermal expansion of Ni-doped MnCoGe at room-temperature magnetic tuning. *ACS Appl Mater Interfaces* 2019;11:17531-8. DOI
14. Shen F, Zhou H, Hu F, et al. Cone-spiral magnetic ordering dominated lattice distortion and giant negative thermal expansion in Fe-doped MnNiGe compounds. *Mater Horizons* 2020;7:804-10. DOI
15. Hu F, Shen B, Sun J, Cheng Z, Rao G, Zhang X. Influence of negative lattice expansion and metamagnetic transition on magnetic entropy change in the compound $LaFe_{11.4}Si_{1.6}$. *Appl Phys Lett* 2001;78:3675-7. DOI
16. Fujita A, Fukamichi K, Wang J, Kawazoe Y. Large magnetovolume effects and band structure of itinerant-electron metamagnetic $La(Fe_xSi_{1-x})_{13}$ compounds. *Phys Rev B* 2003;68:104431. DOI
17. Khmelevskyi S, Mohn P. Theory of invar anomalies in the laves phase RCo_2 ($R = Ho, Dy$) intermetallic compounds. *J Magn Magn Mater* 2004;272-276:525-6. DOI
18. Hu J, Lin K, Cao Y, et al. Adjustable magnetic phase transition inducing unusual zero thermal expansion in Cubic RCo_2-based intermetallic compounds (R = Rare earth). *Inorg Chem* 2019;58:5401-5. DOI
19. Yang N, Dennis K, Mccallum R, Kramer M, Zhang Y, Lee P. Spontaneous magnetostriction in $R_2Fe_{14}B$ (R=Y, Nd, Gd, Tb, Er). *J Magn Magn Mater* 2005;295:65-76. DOI
20. Kuchin A, Medvedeva I, Gaviko V, Kazantsev V. Magnetovolume properties of $Y_2Fe_{17-x}M_x$ alloys (M = Si or Al). *J Alloys Compd* 1999;289:18-23. DOI
21. Cao Y, Lin K, Khmelevskyi S, et al. Ultrawide temperature range super-invar behavior of $R_2(Fe,Co)_{17}$ materials (R = Rare Earth). *Phys Rev Lett* 2021;127:055501. DOI
22. Weiss RJ. The origin of the 'invar' effect. *Proc Phys Soc* 1963;82:281-8. DOI
23. Fang C, Wang J, Hong F, et al. Tuning the magnetic and structural transitions in $TbCo_2Mn_x$ compounds. *Phys Rev B* 2017;96:064425. DOI
24. Bloch D, Lemaire R. Metallic alloys and exchange-enhanced paramagnetism. application to rare-earth-cobalt alloys. *Phys Rev B* 1970;2:2648-50. DOI
25. Duc NH, Goto T. Handbook on the physics and chemistry of rare earths. Amsterdam: Elsevier B.V.; 1999. pp. 1-413.
26. Inishev AA, Gerasimov EG, Mushnikov NV, Terent'ev PB, Gaviko VS. Structure, magnetic and magnetocaloric properties of nonstoichiometric $TbCo_2Mn_x$ compounds. *Phys Met Metallogr* 2018;119:1036-42. DOI
27. Gerasimov E, Inishev A, Mushnikov N, Terentev P, Gaviko V, Anikin M. Magnetocaloric effect, heat capacity and exchange interactions in nonstoichiometric $Er_{0.65}Gd_{0.35}Co_2Mn$ compounds. *Intermetallics* 2022;140:107386. DOI
28. Bentouaf A, Mebsout R, Rached H, Amari S, Reshak A, Aïssa B. Theoretical investigation of the structural, electronic, magnetic and elastic properties of binary cubic C15-Laves phases TbX_2 (X = Co and Fe). *J Alloys Compd* 2016;689:885-93. DOI
29. Gerasimov E, Inishev A, Terentev P, Kazantsev V, Mushnikov N. Magnetostriction and thermal expansion of nonstoichiometric $TbCo_2Mn_x$ compounds. *J Magn Magn Mater* 2021;523:167628. DOI
30. Koley B, Ghanta S, Misra S, Jana PP. Rh_8Cd_{43}: a rhombohedral variant of a cubic giant cell structure. *J Alloy Compd* 2017;695:3760-6. DOI